Supplement to Hector V3.1: functionality and performance of a reduced-complexity climate model

1 Radiative Forcing

Name as it appears in Hector	Description	Source
RF_albedo	surface albedo	externally defined input time series
RF_CO2	CO2 radiative forcing	calculated from concentrations
RF_N2O	N2O radiative forcing	calculated from concentrations
RF_H2O_strat	stratopsheric water vapor radiative forcing	calculated from concentrations
RF_O3_trop	tropsheric ozone radiative forcing	calculated from concentrations
RF_BC	BC radiative forcing	calculated from emissions
RF_OC	OC radiative forcing	calculated from emissions
RF_NH3	NH3 radiative forcing	calculated from emissions
RF_SO2	SO2 radiative forcing	calculated from emissions
RF_aci	radiative forcing from aerosol cloud interactions	calculated from emissions
RF_vol	radiative forcing from volcanic activity	externally defined input time series
RF_misc	radiative forcing from miscellaneous sources	externally defined input time series
FadjCF4	CF4 radiative forcing	calculated from concentrations
FadjC2F6	C2F6 radiative forcing	calculated from concentrations
FadjHFC23	HFC23 radiative forcing	calculated from concentrations
FadjHFC32	HFC32 radiative forcing	calculated from concentrations
FadjHFC4310	HFC4310 radiative forcing	calculated from concentrations

FadjHFC125	HFC125 radiative forcing	calculated from concentrations
FadjHFC134a	HFC134a radiative forcing	calculated from concentrations
FadjHFC143a	HFC143a radiative forcing	calculated from concentrations
FadjHFC227ea	HFC227ea radiative forcing	calculated from concentrations
FadjHFC245fa	HFC245fa radiative forcing	calculated from concentrations
FadjSF6	SF6 radiative forcing	calculated from concentrations
FadjCFC11	CFC11 radiative forcing	calculated from concentrations
FadjCFC12	CFC12 radiative forcing	calculated from concentrations
FadjCFC113	CFC113 radaitive forcing	calculated from concentrations
FadjCFC114	CFC114 radiative forcing	calculated from concentrations
FadjCFC115	CFC115 radiative forcing	calculated from concentrations
FadjCCl4	CCl4 radiative forcing	calculated from concentrations
FadjCH3CCl3	CH3CCl3 radiative forcing	calculated from concentrations
FadjHCFC22	HCFC22 radiative forcing	calculated from concentrations
FadjHCFC141b	HCFC141b radiative forcing	calculated from concentrations
FadjHCFC142b	HCFC142b radiative forcing	calculated from concentrations
Fadjhalon1211	halocarbon 1211 radiative forcing	calculated from concentrations
Fadjhalon1301	halocarbon 1301 radiative forcing	calculated from concentrations
Fadjhalon2402	halocarbon 2402 radiative forcing	calculated from concentrations
FadjCH3Cl	CH3Cl radiative forcing	calculated from concentrations
FadjCH3Br	CH3Br radiative forcing	calculated from concentrations
FCH4	CH4 radiative forcing	calculated from concentrations

SI Table 1: The radiative forcing equations and parameter values are identical to those reported in (Smith et al. 2021) and reproduced here for readers' convenience.

1.1 CO2

Where N and C are atmospheric concentrations at the current timestep of N2O (in ppb) and CO2 (in ppm), respectively, and C0 is the pre-industrial (1850 AD) concentration of CO2 (in ppm), the equations use the following parameterizations.

$$C_{\alpha max} = C_0 - \frac{b_1}{2a_1} \tag{1}$$

$$\alpha' = \begin{cases} d_1 - \frac{b_1^2}{4a_1} & C > C_{\alpha\ max} \\ d_1 + a_1(C - C_0)^2 + b_1(C - C_0) & C_0 < C < C_{\alpha\ max} \\ d_1 & C < C_0 \end{cases} \tag{2}$$

$$\alpha_{N_2O} = c_{1\sqrt{N}} \tag{3}$$

$$SARF_{CO_2} = (\alpha' + \alpha_{N_2O}) ln(C/C_0) \tag{4}$$

$$RF_{CO_2} = \delta_{CO_2} SSARF_{CO_2} + SARF_{CO_2} \tag{5}$$

Equation	**Parameters**	**Value**	**Units**	**Source**
CO_2 Radiative Forcing	a_1	-2.4785e-7	(W m^{-2} ppm^{-2})	Table 7.SM.1(Smith et al. 2021)
CO_2 Radiative Forcing	b_1	7.5906e-4	(W m^{-2} ppm^{-2})	Table 7.SM.1(Smith et al. 2021)
CO_2 Radiative Forcing	c_1	-2.1492e-3	(W m^{-2} $ppb^{-1/2}$)	Table 7.SM.1(Smith et al. 2021)
CO_2 Radiative Forcing	d_1	5.2488	(W m^{-2})	Table 7.SM.1(Smith et al. 2021)
CO_2 Radiative Forcing	δ_{CO_2}	0.05	unitless	7.3.2.3 (Forster, P., T. Storelvmo, K. Armour, W. Collins, J. L. Dufresne, D. Frame, D. J. Lunt, T. Mauritsen, M. D. Palmer, M. Watanabe, M. Wild, H. Zhang 2021)

SI Table 2: Parameter values used to calculate CO_2 radiative forcing.

1.2 N2O

Where *N*, *C*, and *M* are atmospheric concentrations of N_2O (ppb), CO_2 (ppm), and CH_4 (ppb), respectively, and N_0 is the pre-industrial (1850 AD) concentration of N_2O (ppb), the equations use the following parameterizations.

$$SARF_{N_2O} = \left(a_1\sqrt{C} + b_2\sqrt{N} + c_2\sqrt{M} + d_2\right)\left(\sqrt{N} - \sqrt{N_0}\right) \quad (6)$$

$$RF_{N_2O} = \delta_{N_2O} SARF_{N_2O} + SARF_{N_2O} \quad (7)$$

Equation	Parameters	Value	Units	Source
N_2O radiative forcing	a_2	-3.4197e-4	(W m–2 ppm–1)	Table 7.SM.1(Smith et al. 2021)
N_2O radiative forcing	b_2	2.5455e-4	(W m–2 ppb–1)	Table 7.SM.1(Smith et al. 2021)
N_2O radiative forcing	c_2	-2.4357e-4	(W m–2 ppb–1)	Table 7.SM.1(Smith et al. 2021)
N_2O radiative forcing	d_2	0.12173	(W m-2 ppb–1/2)	Table 7.SM.1(Smith et al. 2021)
N_2O radiative forcing	N_0	273.87	ppb	Table 7.SM.1(Smith et al. 2021)
N_2O radiative forcing	δ_{N_2O}	0.05	unitless	7.3.2.3 (Forster et al. 2021)

SI Table 3: Parameter values used to calculate N_2O radiative forcing.

1.3 CH4

Where *N* and *M* are atmospheric concentrations of N_2O (ppb) and CH_4 (ppb), respectively, and M_0 is the pre-industrial (1850 AD) concentration of CH_4, the equations use the following parameterizations.

$$SARF_{CH_4} = \left(a_3\sqrt{M} + b_3\sqrt{N} + d_3\right)\left(\sqrt{M} - \sqrt{M_0}\right) \quad (8)$$

$$RF_{CH_4} = \delta_{CH_4} SARF_{CH_4} + SARF_{CH_4} \quad (9)$$

Equation	Parameters	Value	Units	Source

CH_4 radiative forcing	a_3	-8.9603e-5	W m–2 ppb–1	Table 7.SM.1(Smith et al. 2021)
CH_4 radiative forcing	b_3	-1.2462e-4	W m–2 ppb–1	Table 7.SM.1(Smith et al. 2021)
CH_4 radiative forcing	d_3	0.045194	W m–2 ppb–1/2	Table 7.SM.1(Smith et al. 2021)
CH_4 radiative forcing	δ_{CH_4}	-0.14	unitless	7.3.2.3 (Forster et al. 2021)

SI Table 4: Parameter values used to calculate CH_4 radiative forcing.

1.4 Halocarbons

For a particular Halocarbon species *X*, its radiative forcing is that species's atmospheric concentration, [*X*] (ppt), multiplied by its corresponding radiative efficiency, ρ_X and modified by that species' tropospheric adjustment coefficient, δ_X:

$$SARF_X = \rho_X[X] \tag{10}$$

$$RF_X = SARF_X + \delta_X SARF_X \tag{11}$$

Halocarbon	τ **(lifetime)**	$\rho W\, m^{-2ppt^{-1}}$ **(Radiative efficiency)**	δ **unitless (tropospheric adjustments)**
CF_4	50000.0	0.000099	0
C_2F_6	10000.0	0.000261	0
HFC-23	228.0	0.000191	0
HFC-32	5.4	0.000111	0
HFC-4310	17.0	0.000357	0
HFC-125	30.0	0.000234	0
HFC-134a	14.0	0.000167	0
HFC-143a	51.0	0.000168	0
HFC-227ea	36.0	0.000273	0
HFC-245fa	7.9	0.000245	0
SF_6	3200.0	0.000567	0

CFC-11	52.0	0.000259	0.13
CFC-12	102.0	0.00032	0.13
CFC-113	93.0	0.000301	0
CFC-114	189	0.000314	0
CFC-115	540	0.000246	0
CCl_4	32	0.000166	0
CH_3CCl_3	5	0.000065	0
halon-1211	16.0	0.0003	0
halon-1301	72.0	0.000299	0
halon-2402	28.0	0.000312	0
HCFC-22	11.9	0.000214	0
HCFC-141b	9.4	0.000161	0
HCFC-142b	18.0	0.000193	0
CH_3Cl	0.9	0.000005	0
CH_3Br	0.8	0.000004	0

SI Table 5: Halocarbon parameters from table 7.SM.7 (Smith et al. 2021).

1.5 Aerosols

Direct aerosol radiative forcings for black carbon (BC), organic carbon (OC), SO_2, and NH_3, are modeled as a product of the emissions of that aerosol in that timestep (E; in units of Tg) and the aerosol's specific radiative efficiency, ρ.

$$RF_{BC} = \rho_{BC} E_{BC} \tag{12}$$

$$RF_{OC} = \rho_{OC} E_{OC} \tag{13}$$

$$RF_{SO_2} = \rho_{SO_2} E_{SO_2} \tag{14}$$

$$RF_{NH_3} = \rho_{NH_3} E_{NH_3} \tag{15}$$

51

52 **1.6 Aerosol-cloud Interactions**

$$RF_{aci} = \rho_{aci} ln\left(1 + \frac{E_{SO_2}}{s_{SO_2}} + \frac{E_{BC+OC}}{s_{BC+OC}}\right) \quad (16)$$

53 (16)

Parameter	Value	Units	Source
ρ_{BC}	0.0508	W yr m–2 C Tg–1	7.SM.1.3 of (Smith et al. 2021)
ρ_{OC}	-0.00621	W yr m–2 C Tg–1	7.SM.1.3 of (Smith et al. 2021)
ρ_{SO_2}	-.00000724	W yr m–2 S Gg-1	7.SM.1.3 of (Smith et al. 2021)
ρ_{NH_3}	-.00208	W yr m–2 NH3Tg–1	7.SM.1.3 of (Smith et al. 2021)

54

55 **SI Table 6: Parameter values used to calculate aerosol radiative forcing.**

56 **2 Model Parameterization**

57 Table of the 24 ESM historical output files that were processed to find the global, high latitude, and low latitude mean
58 preindustrial sea surface temperature, which are used by Hector's component.
59

Model	Citation
ACCESS-ESM1-5	(Ziehn et al. 2019a)
CanESM5	(Swart et al., 2019a)
EC-Earth3	(EC-Earth Consortium (EC-Earth), 2019a)
MIROC6	(Tatebe and Watanabe, 2018)
MPI-ESM1-2-HR	(Jungclaus et al., 2019)
MPI-ESM1-2-LR	(Jungclaus et al., 2019)
NorCPM1	(Bethke et al., 2019)
CNRM-CM6-1	(Voldoire, 2018)
CNRM-ESM2-1	(Seferian, 2018)
MIROC-ES2L	(Hajima et al., 2019)
ACCESS-CM2	(Dix et al., 2019a)

AWI-CM-1-1-MR	(Semmler et al., 2018)
CMCC-CM2-HR4	(Scoccimarro et al., 2020)
CMCC-CM2-SR5	(Lovato et al., 2021a)
CMCC-ESM2	(Lovato et al., 2021a)
EC-Earth3-AerChem	(EC-Earth Consortium (EC-Earth), 2020)
EC-Earth3-CC	(EC-Earth Consortium (EC-Earth), 2021)
EC-Earth3-Veg-LR	(EC-Earth Consortium (EC-Earth), 2019b)
MPI-ESM-1-2-HAM	(Neubauer et al., 2019)
MRI-ESM2-0	(Yukimoto et al., 2019a)
NorESM2-LM	(Bethke et al., 2019)
NorESM2-MM	(Seland et al., 2019)
CNRM-CM6-1-HR	(Voldoire, 2018)
EC-Earth3-Veg	(EC-Earth Consortium (EC-Earth), 2019b)

SI Table 7: Table of models and references use to find Hector preindustrial sea surface temperatures.

3 Temperature Component

Figure 1 demonstrates how a user-defined land-ocean warming ratio affects Hector results. Hector's SSP2-45 scenario was run 10 times using land-ocean warming ratios that were uniformly sampled from the (Wallace and Joshi 2018) CMIP5 ensemble range (1.54–1.81). The range in Hector's global (air), land (air), and sea surface mean temperature anomaly results were small over the historical period. In 1950 the model spread is 0.001, 0.026, and 0.007 degrees for global, land, and sea surface temperatures, respectively. This spread increases over the future period and by 2100 the spread is 0.03, 0.49, and 0.11 degrees C for global, land, and sea surface temperatures, respectively. The spread in global temperature is due to carbon-cycle climate interactions.

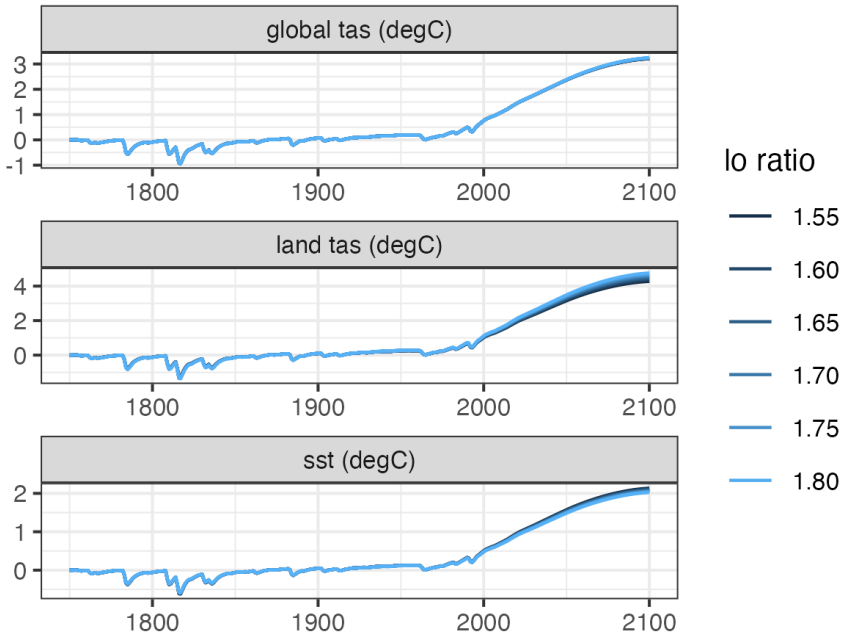

SI Figure 1: Hector global mean air, land air, and sea surface temperature anomalies (degrees C) from 1900 to 2100 for 10 SSP2-45 runs. Each run used a different land-ocean warming ratio sampled from the (Wallace and Joshi 2018) CMIP5 ensemble range (1.54–1.81).

4 CMIP6 Comparison Information

Model	ECS (C)	Citation
ACCESS-CM2	4.7	(Dix et al., 2019b)
ACCESS-ESM1-5	3.9	(Ziehn et al., 2019)
CAMS-CSM1-0	2.3	(Rong, 2019)
CanESM5	5.6	(Swart et al., 2019b)
CESM2	5.2	(Danabasoglu, 2019a)
CESM2-WACCM	4.8	(Danabasoglu, 2019b)
CMCC-CM2-SR5	3.52	(Lovato and Peano, 2020)
CMCC-ESM2	3.57	(Lovato et al., 2021b)
HadGEM3-GC31-LL	5.6	(Good, 2019)

MIROC-ES2L	2.7	(Tachiiri et al., 2019)
MIROC6	2.6	(Shiogama et al., 2019)
MRI-ESM2-0	3.2	(Yukimoto et al., 2019b)
NorESM2-MM	2.5	(Bentsen et al., 2019)
TaiESM1	4.31	(Lee and Liang, 2020)
UKESM1-0-LL	5.3	(Good et al., 2019)

SI Table 8: Summary table of ESM models used to devise the CMIP6 range in Figure 4, the model equilibrium climate sensitivities were obtained from (Schlund et al. 2020), models were categorized according to the IPCC AR6 assessed ranges (Arias et al. 2021).

	Near term, 2021-2004			Mid-term, 2041-2060			Long-term, 2081-2100		
Scenario	Hector	IPCC Best estimate	IPCC Very likely range	Hector	IPCC Best estimate	IPCC Very likely range	Hector	IPCC Best estimate	IPCC Very likely range
ssp119	1.4	1.5	1.2 to 1.7	1.5	1.6	1.2 to 2.0	1.3	1.4	1.0 to 1.8
ssp126	1.4	1.5	1.2 to 1.8	1.7	1.7	1.3 to 2.2	1.6	1.8	1.3 to 2.4
ssp245	1.4	1.5	1.2 to 1.8	1.9	2	1.6 to 2.5	2.5	2.7	2.1 to 3.5
ssp370	1.4	1.5	1.2 to 1.8	2	2.1	1.7 to 2.6	3.4	3.6	2.8 to 4.6
ssp585	1.5	1.6	1.3 to 1.9	2.3	2.4	1.9 to 3.0	4.2	4.4	3.3 to 5.7

SI Table 9: Table of average free running Hector global mean surface temperature anomaly relative to the 1850 to 1900 average compared with values from Table SPM.1 of (IPCC 2021).

References

Bentsen, M., Oliviè, D. J. L., Seland, Ø., Toniazzo, T., Gjermundsen, A., Graff, L. S., Debernard, J. B., Gupta, A. K., He, Y., Kirkevåg, A., Schwinger, J., Tjiputra, J., Aas, K. S., Bethke, I., Fan, Y., Griesfeller, J., Grini, A., Guo, C., Ilicak, M., Karset, I. H. H., Landgren, O. A., Liakka, J., Moseid, K. O., Nummelin, A., Spensberger, C., Tang, H., Zhang, Z., Heinze, C., Iversen, T., and Schulz, M.: NCC NorESM2-MM model output prepared for CMIP6 ScenarioMIP, https://doi.org/10.22033/ESGF/CMIP6.608, 2019.

Bethke, I., Wang, Y., Counillon, F., Kimmritz, M., Fransner, F., Samuelsen, A., Langehaug, H. R., Chiu, P.-G., Bentsen, M., Guo, C., Tjiputra, J., Kirkevåg, A., Oliviè, D. J. L., Seland, Ø., Fan, Y., Lawrence, P., Eldevik, T., and Keenlyside, N.: NCC NorCPM1 model output prepared for CMIP6 CMIP historical, https://doi.org/10.22033/ESGF/CMIP6.10894, 2019.

Danabasoglu, G.: NCAR CESM2 model output prepared for CMIP6 ScenarioMIP, https://doi.org/10.22033/ESGF/CMIP6.2201, 2019a.

Danabasoglu, G.: NCAR CESM2-WACCM model output prepared for CMIP6 ScenarioMIP,

https://doi.org/10.22033/ESGF/CMIP6.10026, 2019b.

Dix, M., Bi, D., Dobrohotoff, P., Fiedler, R., Harman, I., Law, R., Mackallah, C., Marsland, S., O'Farrell, S., Rashid, H., Srbinovsky, J., Sullivan, A., Trenham, C., Vohralik, P., Watterson, I., Williams, G., Woodhouse, M., Bodman, R., Dias, F. B., Domingues, C. M., Hannah, N., Heerdegen, A., Savita, A., Wales, S., Allen, C., Druken, K., Evans, B., Richards, C., Ridzwan, S. M., Roberts, D., Smillie, J., Snow, K., Ward, M., and Yang, R.: CSIRO-ARCCSS ACCESS-CM2 model output prepared for CMIP6 CMIP historical, https://doi.org/10.22033/ESGF/CMIP6.4271, 2019a.

Dix, M., Bi, D., Dobrohotoff, P., Fiedler, R., Harman, I., Law, R., Mackallah, C., Marsland, S., O'Farrell, S., Rashid, H., Srbinovsky, J., Sullivan, A., Trenham, C., Vohralik, P., Watterson, I., Williams, G., Woodhouse, M., Bodman, R., Dias, F. B., Domingues, C. M., Hannah, N., Heerdegen, A., Savita, A., Wales, S., Allen, C., Druken, K., Evans, B., Richards, C., Ridzwan, S. M., Roberts, D., Smillie, J., Snow, K., Ward, M., and Yang, R.: CSIRO-ARCCSS ACCESS-CM2 model output prepared for CMIP6 ScenarioMIP, https://doi.org/10.22033/ESGF/CMIP6.2285, 2019b.

EC-Earth Consortium (EC-Earth): EC-Earth-Consortium EC-Earth3 model output prepared for CMIP6 CMIP historical, https://doi.org/10.22033/ESGF/CMIP6.4700, 2019a.

EC-Earth Consortium (EC-Earth): EC-Earth-Consortium EC-Earth3-Veg model output prepared for CMIP6 CMIP historical, https://doi.org/10.22033/ESGF/CMIP6.4706, 2019b.

EC-Earth Consortium (EC-Earth): EC-Earth-Consortium EC-Earth3-AerChem model output prepared for CMIP6 CMIP historical, https://doi.org/10.22033/ESGF/CMIP6.4701, 2020.

EC-Earth Consortium (EC-Earth): EC-Earth-Consortium EC-Earth-3-CC model output prepared for CMIP6 CMIP historical, https://doi.org/10.22033/ESGF/CMIP6.4702, 2021.

Good, P.: MOHC HadGEM3-GC31-LL model output prepared for CMIP6 ScenarioMIP, https://doi.org/10.22033/ESGF/CMIP6.10845, 2019.

Good, P., Sellar, A., Tang, Y., Rumbold, S., Ellis, R., Kelley, D., Kuhlbrodt, T., and Walton, J.: MOHC UKESM1.0-LL model output prepared for CMIP6 ScenarioMIP, https://doi.org/10.22033/ESGF/CMIP6.1567, 2019.

Hajima, T., Abe, M., Arakawa, O., Suzuki, T., Komuro, Y., Ogura, T., Ogochi, K., Watanabe, M., Yamamoto, A., Tatebe, H., Noguchi, M. A., Ohgaito, R., Ito, A., Yamazaki, D., Ito, A., Takata, K., Watanabe, S., Kawamiya, M., and Tachiiri, K.: MIROC MIROC-ES2L model output prepared for CMIP6 CMIP historical, https://doi.org/10.22033/ESGF/CMIP6.5602, 2019.

Jungclaus, J., Bittner, M., Wieners, K.-H., Wachsmann, F., Schupfner, M., Legutke, S., Giorgetta, M., Reick, C., Gayler, V., Haak, H., de Vrese, P., Raddatz, T., Esch, M., Mauritsen, T., von Storch, J.-S., Behrens, J., Brovkin, V., Claussen, M., Crueger, T., Fast, I., Fiedler, S., Hagemann, S., Hohenegger, C., Jahns, T., Kloster, S., Kinne, S., Lasslop, G., Kornblueh, L., Marotzke, J., Matei, D., Meraner, K., Mikolajewicz, U., Modali, K., Müller, W., Nabel, J., Notz, D., Peters-von Gehlen, K., Pincus, R., Pohlmann, H., Pongratz, J., Rast, S., Schmidt, H., Schnur, R., Schulzweida, U., Six, K., Stevens, B., Voigt, A., and Roeckner, E.: MPI-M MPI-ESM1.2-HR model output prepared for CMIP6 CMIP historical, https://doi.org/10.22033/ESGF/CMIP6.6594, 2019.

Lee, W.-L. and Liang, H.-C.: AS-RCEC TaiESM1.0 model output prepared for CMIP6 ScenarioMIP, https://doi.org/10.22033/ESGF/CMIP6.9688, 2020.

Lovato, T. and Peano, D.: CMCC CMCC-CM2-SR5 model output prepared for CMIP6 ScenarioMIP, https://doi.org/10.22033/ESGF/CMIP6.1365, 2020.

Lovato, T., Peano, D., and Butenschön, M.: CMCC CMCC-ESM2 model output prepared for CMIP6 CMIP historical,

https://doi.org/10.22033/ESGF/CMIP6.13195, 2021a.

Lovato, T., Peano, D., and Butenschön, M.: CMCC CMCC-ESM2 model output prepared for CMIP6 ScenarioMIP, https://doi.org/10.22033/ESGF/CMIP6.13168, 2021b.

Neubauer, D., Ferrachat, S., Siegenthaler-Le Drian, C., Stoll, J., Folini, D. S., Tegen, I., Wieners, K.-H., Mauritsen, T., Stemmler, I., Barthel, S., Bey, I., Daskalakis, N., Heinold, B., Kokkola, H., Partridge, D., Rast, S., Schmidt, H., Schutgens, N., Stanelle, T., Stier, P., Watson-Parris, D., and Lohmann, U.: HAMMOZ-Consortium MPI-ESM1.2-HAM model output prepared for CMIP6 CMIP historical, https://doi.org/10.22033/ESGF/CMIP6.5016, 2019.

Rong, X.: CAMS CAMS-CSM1.0 model output prepared for CMIP6 ScenarioMIP, https://doi.org/10.22033/ESGF/CMIP6.11004, 2019.

Scoccimarro, E., Bellucci, A., and Peano, D.: CMCC CMCC-CM2-HR4 model output prepared for CMIP6 CMIP historical, https://doi.org/10.22033/ESGF/CMIP6.3823, 2020.

Seferian, R.: CNRM-CERFACS CNRM-ESM2-1 model output prepared for CMIP6 CMIP historical, https://doi.org/10.22033/ESGF/CMIP6.4068, 2018.

Seland, Ø., Bentsen, M., Oliviè, D. J. L., Toniazzo, T., Gjermundsen, A., Graff, L. S., Debernard, J. B., Gupta, A. K., He, Y., Kirkevåg, A., Schwinger, J., Tjiputra, J., Aas, K. S., Bethke, I., Fan, Y., Griesfeller, J., Grini, A., Guo, C., Ilicak, M., Karset, I. H. H., Landgren, O. A., Liakka, J., Moseid, K. O., Nummelin, A., Spensberger, C., Tang, H., Zhang, Z., Heinze, C., Iversen, T., and Schulz, M.: NCC NorESM2-LM model output prepared for CMIP6 CMIP historical, https://doi.org/10.22033/ESGF/CMIP6.8036, 2019.

Semmler, T., Danilov, S., Rackow, T., Sidorenko, D., Barbi, D., Hegewald, J., Sein, D., Wang, Q., and Jung, T.: AWI AWI-CM1.1MR model output prepared for CMIP6 CMIP historical, https://doi.org/10.22033/ESGF/CMIP6.2686, 2018.

Shiogama, H., Abe, M., and Tatebe, H.: MIROC MIROC6 model output prepared for CMIP6 ScenarioMIP, https://doi.org/10.22033/ESGF/CMIP6.898, 2019.

Swart, N. C., Cole, J. N. S., Kharin, V. V., Lazare, M., Scinocca, J. F., Gillett, N. P., Anstey, J., Arora, V., Christian, J. R., Jiao, Y., Lee, W. G., Majaess, F., Saenko, O. A., Seiler, C., Seinen, C., Shao, A., Solheim, L., von Salzen, K., Yang, D., Winter, B., and Sigmond, M.: CCCma CanESM5 model output prepared for CMIP6 CMIP historical, https://doi.org/10.22033/ESGF/CMIP6.3610, 2019a.

Swart, N. C., Cole, J. N. S., Kharin, V. V., Lazare, M., Scinocca, J. F., Gillett, N. P., Anstey, J., Arora, V., Christian, J. R., Jiao, Y., Lee, W. G., Majaess, F., Saenko, O. A., Seiler, C., Seinen, C., Shao, A., Solheim, L., von Salzen, K., Yang, D., Winter, B., and Sigmond, M.: CCCma CanESM5 model output prepared for CMIP6 ScenarioMIP, https://doi.org/10.22033/ESGF/CMIP6.1317, 2019b.

Tachiiri, K., Abe, M., Hajima, T., Arakawa, O., Suzuki, T., Komuro, Y., Ogochi, K., Watanabe, M., Yamamoto, A., Tatebe, H., Noguchi, M. A., Ohgaito, R., Ito, A., Yamazaki, D., Ito, A., Takata, K., Watanabe, S., and Kawamiya, M.: MIROC MIROC-ES2L model output prepared for CMIP6 ScenarioMIP, https://doi.org/10.22033/ESGF/CMIP6.936, 2019.

Tatebe, H. and Watanabe, M.: MIROC MIROC6 model output prepared for CMIP6 CMIP historical, https://doi.org/10.22033/ESGF/CMIP6.5603, 2018.

Voldoire, A.: CMIP6 simulations of the CNRM-CERFACS based on CNRM-CM6-1 model for CMIP experiment historical, https://doi.org/10.22033/ESGF/CMIP6.4066, 2018.

Yukimoto, S., Koshiro, T., Kawai, H., Oshima, N., Yoshida, K., Urakawa, S., Tsujino, H., Deushi, M., Tanaka, T., Hosaka,

M., Yoshimura, H., Shindo, E., Mizuta, R., Ishii, M., Obata, A., and Adachi, Y.: MRI MRI-ESM2.0 model output prepared for CMIP6 CMIP historical, https://doi.org/10.22033/ESGF/CMIP6.6842, 2019a.

Yukimoto, S., Koshiro, T., Kawai, H., Oshima, N., Yoshida, K., Urakawa, S., Tsujino, H., Deushi, M., Tanaka, T., Hosaka, M., Yoshimura, H., Shindo, E., Mizuta, R., Ishii, M., Obata, A., and Adachi, Y.: MRI MRI-ESM2.0 model output prepared for CMIP6 ScenarioMIP, https://doi.org/10.22033/ESGF/CMIP6.638, 2019b.

Ziehn, T., Chamberlain, M., Lenton, A., Law, R., Bodman, R., Dix, M., Wang, Y., Dobrohotoff, P., Srbinovsky, J., Stevens, L., Vohralik, P., Mackallah, C., Sullivan, A., O'Farrell, S., and Druken, K.: CSIRO ACCESS-ESM1.5 model output prepared for CMIP6 ScenarioMIP, https://doi.org/10.22033/ESGF/CMIP6.2291, 2019.